Fuel 312 (2022) 122851

Contents lists available at ScienceDirect

Fuel

journal homepage: www.elsevier.com/locate/fuel

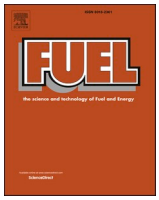

Full Length Article

Study on the migration and structure evolution of the carbon in the slag layer and its effect on the coal slag transformation

Xiaodan Bao [a], Ming Gong [b], Zhongjie Shen [a,*], Jianliang Xu [a], Qinfeng Liang [a], Haifeng Liu [a]

[a] Shanghai Engineering Research Center of Coal Gasification, East China University of Science and Technology, P. O. Box 272, Shanghai 200237, PR China
[b] Quality Supervision and Inspection of Building and Sanitary Ceramics of Jiangxi Province, Gao An, Jiangxi 330800, PR China

ARTICLE INFO

Keywords:
Entrained flow gasifier
Rheology
Residual carbon
Structure evolution
Slag transformation

ABSTRACT

The carbon remained/covered in the molten slag layer changes the chemical and physical properties in the entrained flow gasifier and further affects the slag rheology. Our current study focused on the migration and structure evolution of the carbon in the coal slag layer. Besides, the effect of the carbon on the slag transformation was studied as well. The experimental results showed that part of the carbon migrated upward to the molten slag surface during the heating and isothermal process due to its lower density, while the rest reacted with the molten slag or remained as the residual carbon. During the migration process, the iron oxide was reduced to metallic iron enclosure by the carbon via the carbothermal reaction. Both the mass ratio of the carbon that consumed by the slag to initial carbon layer and the carbon capacity of the molten slag increased with the increases of the temperature and residence time. In addition, Raman spectroscopy was used to characterize the structure evolution of the residual carbon. The results showed that with the increase of the slag temperature and residence time, the disordered degree of the residual carbon structure increased and the intensity of the ideal graphite lattice decreased, which promoted the occurrence of the carbothermal reaction. Finally, comparing the carbon migration layer to the non-carbon layer, it was found that the migration, carbothermal reaction, and structure evolution of the carbon promoted the mineral transformation and crystallization behavior of the slag layer.

1. Introduction

The entrained flow coal gasification technology with its competitively low-cost advantage to produce syngas (e.g. H_2 and CO) is widely used in the fields of chemical production, fuel cell, and power generation [1]. This technology uses pulverized coal or coal water slurry to react with the gasification agents (water vapor, oxygen, etc.) to produce syngas [2–3]. Minerals in the coal convert to coal ash or melted to slag, and some of which deposit on the wall of the gasifier and flow down through the slag tap hole [4–5]. In the entrained flow gasifier, partially-gasified coal/char particles carried by the gas flow will deposit on the wall, and this amount accounts for about 55.4% injected coal particles from a study of Xu et al. [6]. Approximately 22.5% of the captured coal/char particles continued to react with near-wall gases while the rest part remained in the molten slag layer. The unreacted carbon particles, gases, and coal ash and slag particles on the gasifier wall accumulate to form a complex environment, and the interactions among these further affect the rheology of the slag layer. Thus, the evolution of the carbon embedded/remained in the molten slag layer is essential to the slag discharge of an entrained flow gasifier.

Ni et al. [7] proposed a submodel considering the influence of viscosity, surface tension, impacting angle and velocity on the wall deposition of particles in the slagging system. The results showed that the deposition probability of large slag particles was higher than small particles, which increased with the increase of melting temperature. Comparatively, Safronov et al. [8] developed a steady-state model that coupled the slag model with the CFD-based reactor model, to describe the slag flow and heat transfer characteristics in the entrained flow gasifier. A variation of the two-layer approach considering the boundary between solid and liquid slag layers where the slag temperature was the temperature of critical viscosity (T_{cv}) was applied in the model. Interactions between the operating conditions, liquid and solid slag layer thicknesses, and the main gasification parameters were analyzed. Generally, the results of the interaction between char particles and slag wall include three patterns, including entrapment, segregation, and coverage, from the studies of Montagnaro et al. [9,10]. Char particles

* Corresponding author.
E-mail address: zjshen@ecust.edu.cn (Z. Shen).

https://doi.org/10.1016/j.fuel.2021.122851
Received 24 October 2021; Received in revised form 27 November 2021; Accepted 4 December 2021
Available online 11 December 2021

Table 1
The proximate and ultimate analyses of the coal and coal char sample (air-dried basis, wt.%) used in this study.

	Proximate analysis (wt. %)				Ultimate analysis (wt. %)				
Components	M_{ad}	V_{ad}	FC	A_{ad}	C	H	O	S	N
Raw coal	11.98	37.93	36.02	14.04	49.04	3.49	17.89	2.01	1.52
Coal Char	1.62	3.61	71.89	22.88	68.08	1.85	2.76	1.98	0.8

deposited on the wall of the entrained flow gasifier continued to react with the near-wall gas. From our previous studies [11–13], the gasification reaction of the captured char particles was promoted while the combustion on the char-slag interface was inhibited. Once a char particle deposited on the slag surface, its residence time was prolonged in the gasifier. In addition, the high-temperature surface of the slag wall benefitted from the gasification reaction. The promoting effect of the coal ash and slag on the gasification reaction, including the catalytic function from alkali or alkaline earth metals (AAEMs), was also verified by Li et al. [14] through experiments. Thus, the vast majority of captured char particles in an entrained flow gasifier are converted to syngas during a wall reaction [6]. However, part of the captured char particles was embedded or immersed by the flowing molten slag and transformed to the residual carbon. Due to the isolated environment in the molten slag layer, the combustion or gasification of char particles with near-wall gases was prevented. The residual carbon in the molten slag layer, as solid phase, proved to affect the slag viscosity and flow ability [15]. Additionally, the carbon would react with the slag via carbothermal reaction and change the chemical composition [16], affecting the chemical and physical properties of the slag layer.

Researchers found that the addition of the residual carbon increased the melting temperature of the coal ash and slag [16,17]. Under the condition of unstable gasifier operation (e.g. insufficient oxygen supply), the carbon content of fine slag and coarse slag can reach 60% and 30–35% respectively [18,19]. Wang et al. [20] found that the graphitization degree of residual carbon in ash residue of anthracite mobile bed gasification is higher than that of raw coal pyrolytic char. The graphitization degree referred to the degree to which the carbon atoms form a close-packed hexagonal graphite crystal structure. Minerals would react with carbon at high temperature. Kong et al. [15] found that Si-O bonds in quartz (SiO_2) were more likely to react with carbon than Si-O bonds in Ca-Al-Si-O and Ca-Si-O systems, and there was a competitive relationship between the reaction of silicon-containing minerals and residual carbon. Ma et al. [21,22] found that mullite reacted with the coal char in the inert atmosphere (Ar) to form silicon carbide (SiC) and corundum (Al_2O_3) at 1500 ℃. However, this reaction was inhibited in the CO atmosphere, and the graphitization degree of the residual carbon was not conducive to the occurrence of the carbothermal reaction [16]. Wang et al. [23] studied the carbothermal reaction of minerals with coal char in the inert atmosphere, of which the carbothermal reactions of quartzite, mullite and calcium oxide with coal char occurred at 1200 ℃, 1150 ℃, and 1450 ℃, respectively. Moreover, the SiO_2/Al_2O_3 ratio in the coal ash mainly affected the carbothermal reaction of Si and C, and the carbon consumption rate decreased first and then increased with the SiO_2/Al_2O_3 ratio [24]. For Fe_2O_3 in the coal slag, the increasing content improved the reaction temperature, degree, and reaction rate [25]. From the abovementioned studies, it was found that the migration and evolution of the carbon from the embedded coal/char particles in the slag layer have not been clearly explained, and using graphite to study the evolution of coal char and its interaction with slag cannot fully reveal the real process and reaction in the entrained flow gasifier.

Table 3
The ash fusion temperatures (AFTs) of the coal ash samples in this study.

AFTs	DT (℃)	ST (℃)	HT (℃)	FT (℃)
SF coal ash	1138	1147	1158	1184
XLT coal ash	1307	1366	1375	1379

In this study, the migration and structure evolution of the carbon in the molten slag layer was investigated. The mass ratio of the carbon that consumed by the molten slag and the carbon capacity of the molten slag with the effects of residence time period and slag layer temperature were quantitively investigated as well. The structure of the residual carbon during the migration process in the molten slag layer was analyzed via Raman spectroscopy to reveal the evolution rule. The effect of the carbon on the slag transformation was studied, including the comparison of the carbon-containing layer and non-carbon layer.

2. Experimental

2.1. Materials

The coal char sample used in this study was prepared from a Chinese coal named Xiaolongtan (XLT) lignite coal in a drop tube furnace at 1350 ℃ under an argon atmosphere. The length of the drop tube furnace is totally 2.2 m. This drop tube furnace has a 1.2 m length high-temperature zone. The flowrate of the argon gas was set to 1.2 L/min in this study, which was based on the setting parameters from the manufacturer, to keep a stable gas flow and remove the air inside. The feeding rate of the solid material from the manufacturer ranges from 2.0 to 4.0 g/min to keep a stable particle flow. In this study, the coal feeding rate was set to 3.33 g/min. The proximate and ultimate analyses of the coal and coal char sample are tested and the results are given in Table 1.

In this study, a coal ash sample with a low flow temperature was used to create a molten slag environment. This coal ash sample was prepared from a bituminous coal (Shenfu Coal) in a N17/HR-K muffle furnace (Nabertherm Company, Lilienthal, Germany) at 815 ℃, which was heated to 815 ℃ and held for 2 h. The coal sample was fully reacted with air in the furnace and converted to gas and coal ash. The chemical compositions of SF coal ash and XLT coal ash were analyzed by Advant'X Intellipower^{TM} 3600 X-ray fluorescence (XRF, Thermo Fisher Scientific, America). The chemical compositions of the two coal ash samples are shown in Table 2. The ash fusion temperatures (AFTs) were tested by a 5E-AF4000 ash fusion point determination meter (Kaiyuan Company, Changsha, China). AFTs include the deformation temperature (DT), softening temperature (ST), hemispherical temperature (HT), and flow temperature (FT) [26]. DT means the deformation temperature where first rounding of the ash cone tip is taking place. ST is the softening or sphere temperature where the cone height is equal to the cone width. HT means the hemispherical temperature where cone height is equal to 1/2 cone width. Fluid or flow temperature (FT) is the temperature where the

Table 2
Chemical compositions (wt.%) of the coal ash samples.

Component	SiO_2	Al_2O_3	Fe_2O_3	CaO	K_2O	TiO_2	MgO	Na_2O	SO_3
SF	47.31	19.44	9.98	17.03	1.05	0.70	1.29	2.40	0.81
XLT	22.10	15.88	12.02	23.05	0.70	0.75	3.82	0.36	20.74

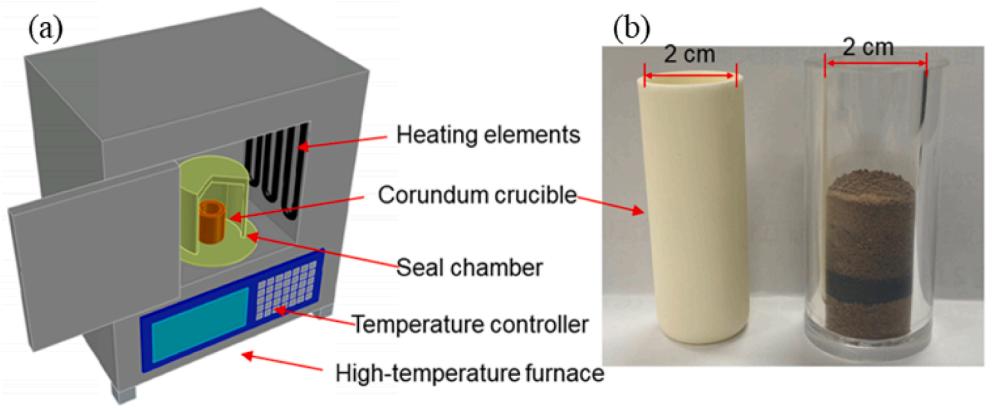

Fig. 1. The schematic diagram of the high-temperature furnace (a) and sample placement (b).

cone height is equal to 1.6 mm. The AFTs of SF coal ash and XLT coal ash were 1184 °C and 1379 °C, as shown in Table 3. Due to the high flow temperature of XLT coal ash and the residual carbon would increase the AFTs [17], this coal ash with coal char cannot be melted in the high-temperature furnace from the primary experiment. Therefore, SF coal ash was used to be melted as the molten slag layer in this study.

2.2. Experimental method

To study the migration and structure evolution of the carbon in the molten slag layer, a simulation experiment was carried out in the high-temperature furnace of Fig. 1a. A coal char layer (1.20 g) was buried in the coal ash layer (10.00 g) in a crucible, which is shown in Fig. 1b. The carbon content of XLT coal char is 68.08 wt% in Table 1. Then, the carbon contents in the coal char and coal ash mixtures were calculated and the residual carbon content in the simulated sample was about 7.29 wt%. The analytical data from the published work by Pan et al. [27] pointed out that the residual carbon content in the coarse slag ranged from 2.54 to 7.43 wt% in an industrial entrained flow gasifier. In addition, researches on the residual carbon from studies [18,28] showed that the residual carbon from the coarse slag of a commercial entrained flow gasifier ranged 3.0 to 20.95 wt%. Thus, the carbon content used in this study was acceptable and close to the value from the industrial entrained flow gasifier. To show the position of the char particle layer in the slag layer, a plexiglass crucible was used in Fig. 1b instead of the corundum crucible (Φ23.00 × 58.00 mm). The black layer is the coal char layer and the brown layer is the coal ash layer. The corundum crucible (purity 99.9% Al_2O_3) was used in the actual experiment.

To prevent the reaction of char particles with air, the corundum crucible was placed in the seal chamber with graphite inside. The graphite reacted with air in the seal chamber to create a reducing atmosphere, to simulate the real environment of the entrained flow gasification process. In an entrained flow gasifier, the composition of the gas atmosphere and the oxygen partial pressure at the slag wall cannot easily be determined. As Schwitalla et al. [29] did the work that they used FactSage software to calculate oxygen partial pressure on slag wall, the calculated oxygen partial pressure was between 10^{-15} and 10^{-13} bar between 1200 and 1450 ℃. Similar measures have been taken in the past in order to include the effect of the gas atmosphere on slag behavior [30,31]. The mass of graphite was much more than the amount of O_2 in the air to be consumed because there was still some graphite around the crucible after the experiment. Therefore, the graphite around the crucible consumed O_2 in the seal chamber to create a reducing atmosphere.

The crucible in the high-temperature furnace was heated up to different temperatures (1300 ℃, 1350 ℃, 1400 ℃, and 1450 ℃), and held for different residence time periods (0, 15, 30 and 60 min). In this study, the heating rate was set to 15 ℃/min when the temperature was below 1200 ℃. After that, the heating rate was changed to 5 ℃/min, and then the temperature was rose to the set value. This heating procedure was set based on the standard operating procedure for protecting the heating elements. In this study, each crucible that contained char particle layer and slag layer was heated up to a temperature continuously (e.g. 1300 ℃) and remained at this temperature for a residence time period (e.g. 0 min). Then, the slag sample was cool down slowly and naturally. The cooling rate calculated based on the set temperature and time was about 10 ℃/min. The experiment for char particles at different residence time periods embedded in the molten slag was to study the transformation of the residual carbon during the slag flow process in the entrained flow gasifier. Char particles were completely embedded in the molten slag, while other char particles without slag contact or on the surface from the beginning to end were not considered. The study on the effect of the temperature was to evaluate the migration and structure evolution of the carbon and slag at different wall zones with different temperatures.

After it cooled down, the crucible was axially cut to get the cross section by a cutter (TechCut 4^{TM}, Allied High Tech. Products. Inc., America) for analysis. The cutting process used a coolant (e.g. water) to allow the sample to be at room temperature. The cutting speed of the saw was set to 120 RPM. At room temperature, the structures of coal char and slag would not be changed. One part was then cut into a 1 mm thick slice and this 1 mm thick slice was put on conducting glue, which was then coated with gold vapor to make the sample conductive. The morphologies and elemental distribution and composition of samples were analyzed by a scanning electron microscope (SU1510 SEM, Hitachi, Japan) with combined an energy dispersive spectroscopy (EDS, Hitachi, Japan). The rest samples were ground to powder using a vibrating ball mill (Retsch, Germany). It works at room temperature and the sample being milled is held at low temperature. The powder has a particle size of 1–10 μm, which preserved the lattice of minerals present in the sample [32]. XRD patterns of samples were acquired by a PANalytical X'pert Powder X-ray powder diffractometer with Cu Kα radiation. The operating conditions were 40 kV and 40 mA. The samples were scanned from 2θ = 10–80° with 0.01° step size. Crystalline minerals were further analyzed using Jade 6.5 software based on the XRD patterns of the samples. In addition, Raman spectroscopy (ThermoFisher Scientific, America) was used to analyze the structure of the cooled sample under different experimental conditions.

2.3. Mathematical calculation

Due to the lower density of the char particle than the slag and the effect of buoyancy, part of char particles gradually floated up to the slag surface in this study. Although the graphite in the seal chamber reacted with air to create a reducing atmosphere, it was possible that small part of char particles on the slag surface continued to react with air in the seal chamber. Therefore, during the migration process of char particles, four

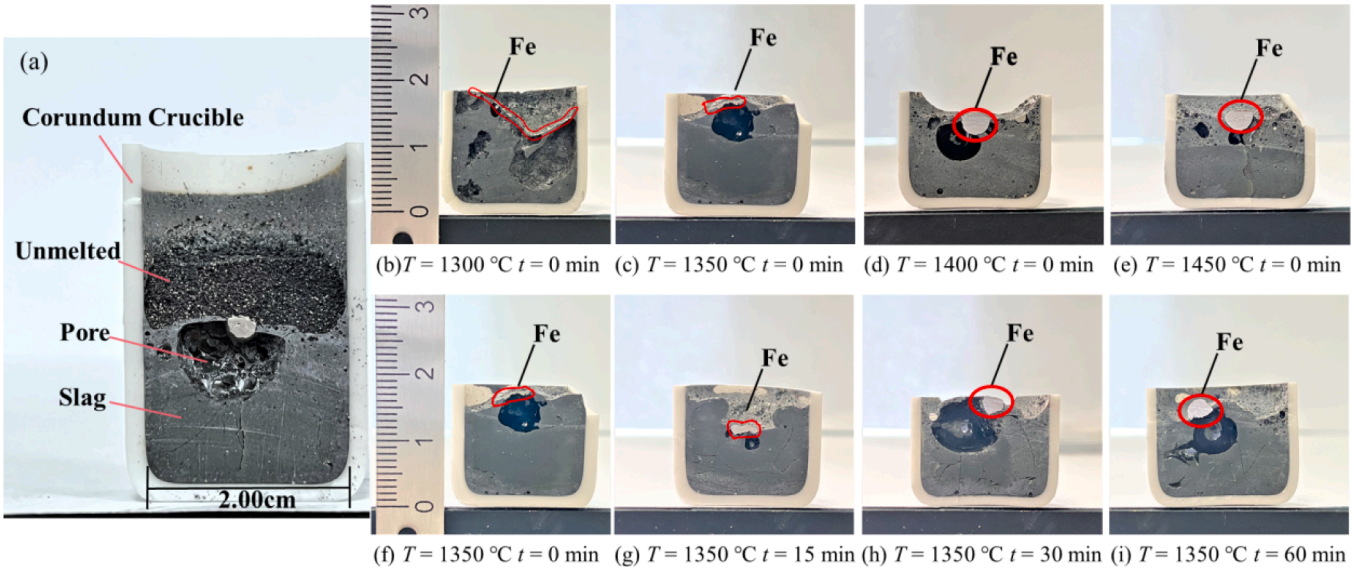

Fig. 2. Photos of the cross sections of the crucible, slag sample, and residual carbon layer at different temperatures and residence time periods.

scenarios occurred and included the carbothermal reaction with the molten slag, remain in the molten slag, floating on the molten slag surface, and the reaction with air. Char particles in the former two scenarios were consumed by the molten slag while char particles in the latter two scenarios floated up to the slag surface.

In this study, the mass ratio of the carbon in char particles that consumed by the molten slag to the total carbon in the char sample layer was defined to characterize the escape ability of the carbon reversely. This mass ratio directly reflected the amount of the carbon embedded in the slag layer that was able to migrate away and continue to react with the outside gas in the entrained flow gasifier. The carbon that consumed by the molten slag included both carbon amount via carbothermal reaction with the molten slag and remain in the molten slag. Thus, the defined mass ratio in this study can be expressed as:

$$w_c = \frac{m_{cc}}{m_{tc}} \tag{1}$$

where w_c was the mass ratio, m_{cc} was the mass of the carbon that consumed by the molten slag, kg, and m_{tc} was the total mass of the carbon in the char sample layer, kg. During the heating process, the initial contents of moisture and volatiles in Table 1 were low and they experienced high-temperature processes and would be less during the char migration process. Thus, for the char particles under these four scenarios, the carbon content was assumed the same in char particles

$$m_{cc} = m_{cp} \bullet \varphi_c \tag{2}$$

$$m_{tc} = m_{c0} \bullet \varphi_c \tag{3}$$

where m_{cp} was the mass of char particles that consumed by the molten slag, kg, φ_c was the carbon content of the char sample, wt.%, and m_{c0} was the total mass of the char sample layer in the slag, kg. In this study, the total mass of the char sample layer was 1.2 g. Then, substituting Eqs. (2) and (3) to Eq. (1), Eq. (1) can be rewritten as:

$$w_c = \frac{m_{cp}}{m_{c0}} \tag{4}$$

Second, a carbon capacity of the molten slag was defined to quantitively analyze the ability of the molten slag per unit mass that reacted with the carbon or remain inside, which was essential to the physical and chemical properties of the slag layer. The carbon that consumed by the molten salg converted to gases (e.g. CO or CO_2) and other compounds, such as Fe_3C. The carbon capacity of the molten slag was calculated as the mass ratio of the carbon that consumed by the molten slag, including both carbons reacted with the molten slag and remained in the molten salg, to the mass of the molten slag. The carbon capacity was denoted and calculated as:

$$I_c = \frac{m_{cc}}{m_s} \tag{5}$$

where I_c was the carbon capacity, kg/kg, and m_s was the mass of the slag, kg. The mass of the slag (m_s) was equal to the sum of the initial coal ash mass and the ash mass of char particles that consumed by the slag with both removing the mass of SO_2. In this study, 1.2 g coal char sample was used and the SF coal ash sample was set to 10.0 g. From Tables 1 to 2, XLT coal char contains 22.88 wt% ash and the SO_3 content in the coal ash is 20.74 wt%. SF coal ash contains 0.81 wt% SO_3. Anhydrite would disappear with higher residence time periods and higher temperatures. Thus, the released gas from the mineral decomposition was assumed as SO_2. The SO_2 weight fraction was calculated as 0.9 wt% released from the mixed sample. The coal ash in the char layer added to the SF coal ash was about 0.233 g. The mass addition of the coal ash of char particles and the mass loss of SO_2 were small compared to the initial ash layer.

The total mass of the char sample layer in Eq. (4) was equal to the sum of the mass of char particles that consumed by the molten slag and the mass of un-consumed char particles on the slag surface, namely

$$m_{c0} = m_{cp} + m_{ucp} \tag{6}$$

In Eq. (6), m_{ucp} was the mass of un-consumed char particles, which contained one part that floated on the slag surface, as shown in Fig. 2a, and the other part that reacted with air.

$$m_{ucp} = m_{cf} + m_{ca} \tag{7}$$

where m_{cf} was the mass of char particles floated on the slag surface but not reacted with air and slag, kg, and m_{ca} was the mass of char particles that reacted with air, kg. From the experimental results shown in Fig. 2a, there was an unmelted particle layer on the slag surface after it cooled down. Note that the mass of this unmelted particel layer was not excactly equal to the total mass of un-consumed char particles floated up to the moteln slag surface, due to the further reaction of floating char particles with air. The other part that reacted with air would leave ash and further combined char particles floated on the slag surface (m_{cf}) to an unmelted layer. Then, the mass of the unmelted layer, denoted as m_{ul}, kg, was expressed as:

$$m_{ul} = m_a + m_{cf} \tag{8}$$

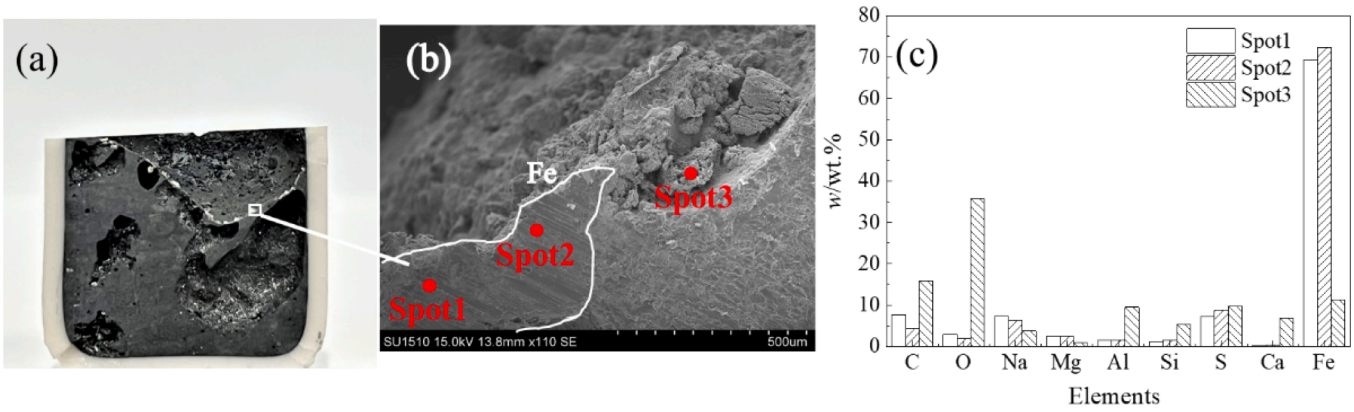

Fig. 3. The cross section (a) and SEM image (b) of the slag sample and EDS analysis (c) at 1300 ℃ for the residence time period of 0 min.

In Eqs. (8) and (9), m_a was the mass of the ash after char particle reacted with air and remained in the unmelted particle layer, kg. In this study, it was difficult to directly determine the mass of char particles that reacted with air during the experiment. However, according to the mass conservation of the coal ash before and after the experiment, the total mass of the ash in the un-consumed particle layer could be measured by using a combusted weight loss method. Since the composition change in the ash compsition differed in the reducing and oxidizing atmosphere, FactSage software was used to calculate the thermochemical equilibrium of the ash based on the method in Ref. [33]. The weight loss difference between these two atmospehres was calcualted about 0.5 to 0.7%, which was added in the calculation. The experiment was carried out in the high-temperature furnace as well. Thus, the mass of the unmelted particle layer was actually the sum of the total ash mass and the lost weight mass during the combusted weight loss experiment

$$m_{ul} = m_{ta} + \Delta m \tag{9}$$

and

$$m_{ta} = m_{ucp} \bullet \varphi_a \tag{10}$$

where Δm was the weight loss of the unmelted particle layer before and after the combustion experiment in the high-temperature furnace, kg. m_{ta} was the total mass of the ash in the unmelted particle layer, kg, and φ_a was the ash content of the char particle. m_{ul} can be measured after the experiment of the carbon migration. The coal ash content (φ_a) of the char sample was known and given in Table 1. Thus, combining Eqs. (9) to (10), the mass of char particles that un-consumed by the molten slag (m_{ucp}) was calculated as

$$m_{ucp} = \frac{m_{ta}}{\varphi_a} = \frac{m_{ul} - \Delta m}{\varphi_a} \tag{11}$$

Then, substituting Eqs. (6) and (11) to Eq. (4), the mass ratio of the carbon that consumed by the molten slag to the total carbon in the char sample layer can be calculated as:

$$w_c = 1 - \frac{m_{ul} - \Delta m}{m_{c0}} \bullet \frac{1}{\varphi_a} \tag{12}$$

and substituting Eqs. (2), (6), and (11) to Eq. (5), carbon capacity was calculated as

$$I_c = \frac{m_{c0}}{m_s} \bullet \varphi_c - \frac{m_{ul} - \Delta m}{m_s} \bullet \frac{\varphi_c}{\varphi_a} \tag{13}$$

3. Results and discussion

3.1. Carbon migration in the molten slag layer

Fig. 2 shows photos of the cross sections of corundum crucibles with cooled slag samples from the experiments at different temperature and residence time periods. From Fig. 2a, it was clearly found that pores, unmelted coal ash/char, and melted slag were on the cross section. During the coal ash melting and isothermal process, char particles migrated to the slag surface and finally formed a dense particle layer on the molten slag surface. The formation of the pore was speculated to form from bubbles due to the product gas (e.g. CO or CO_2) from the carbothermal reaction between the char particle and molten slag. Carbon reacted with the oxides (e.g. FeO) in the molten slag and converted to CO or CO_2. These gases diffused into the liquid slag and bubbles formed. From Fig. 2b to 2e, when the residence time period at the set temperature was 0 min, the distribution of pores on the cross section changed with the increase of the isothermal temperature. When the temperature was 1300 ℃, pores had a large size and were dispersed throughout the cross section of the cooled slag. When the temperature increased to 1450 ℃, bubbles moved the slag surface and the size decreased. According to Stokes' law [34], smaller bubbles had lower rising speeds while the velocity of the larger bubble was higher, and hence larger pores were found close to the slag surface in Fig. 2. Smaller pores were found randomly distributed in the slag layer. Besides, the viscosity of the slag decreased drastically at higher temperatures, which made it easier for the bubbles to escape the slag. This indicated that the residual carbon was mainly distributed in slag layer at low temperature. When the temperature rose, the increasing temperature reduced the slag viscosity and enhanced the flow ability, owing to the lower density, the residual carbon gradually migrated to the slag surface. When the temperature was set to 1350 ℃ from Fig. 2f to 2i, the distribution of the pores was close to the slag surface but pores had different sizes at different residence time periods.

Additionally, the left photo (Fig. 2a) also displayed a metallic particle formed on the edge between the pore and the unmelted char particle layer. The metallic enclosure can be found at all tested conditions in Fig. 2, which was also found in real gasifiers [29]. When the isothermal temperature of the molten slag increased from 1300 ℃ to 1450 ℃, the shape of the metallic enclosure changed from banded to granular. The results were found from Fig. 2f to 2i when the residence time period increased.

To determine the chemical composition of the metallic enclosure, a scanning electron microscope combined with an energy dispersive spectrometer was used to analyze the chemical compositions of the slag and metallic enclosure, and the results are given in Fig. 3. The photo in Fig. 3b was captured from Fig. 3a, which was the cross section of the crucible and cooled slag. From Fig. 3b, spots 1 and 2 were on the metallic enclosure while spot 3 was on the slag. The analytical results in Fig. 3c showed that the main composition on spots 1 and 2 was metallic Fe with the contents of about 70% to 80%. On the spot 3, the main chemical compositions were C, O, Al, Si, S, and Ca. Therefore, it was concluded that the metallic enclosure was metallic Fe reduced from the iron oxides

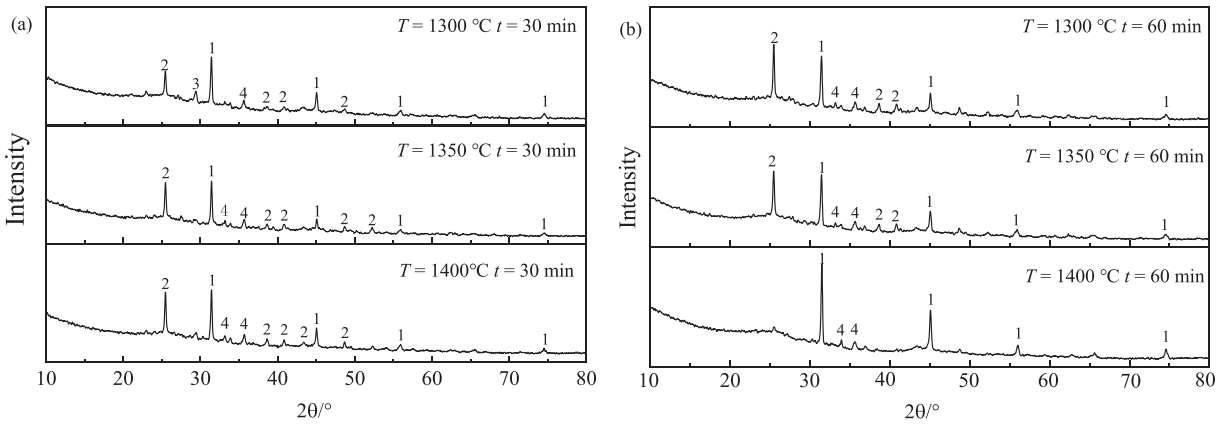

Fig. 4. XRD spectra of the unmelted samples at different temperatures (a) and different residence time periods (b). (1-Oldhamite (CaS), 2-Anhydrite ($CaSO_4$), 3-Calcite ($CaCO_3$), 4-Hematite (Fe_2O_3)).

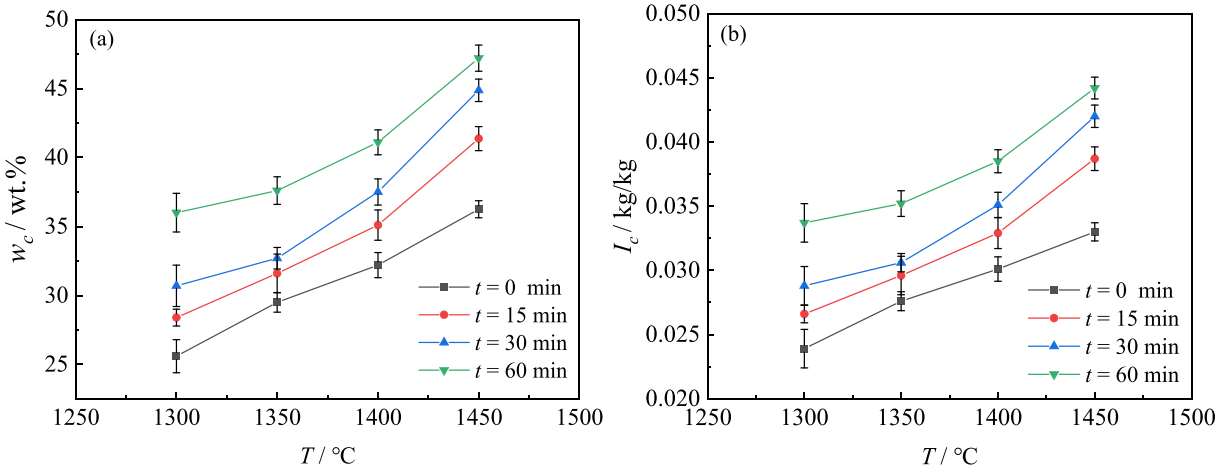

Fig. 5. The mass ratio (w_c) of the carbon that consumed by the molten slag to the total carbon in the char sample layer (a) and carbon capacity (I_c) of the molten slag at different temperatures (b).

of the slag by residual carbon during the migration process as Eq. (I), which was found in Ref. [25] that the slag block containing metal iron appeared at the outlet of a gasifier. Similar phenomenon was found in a moving bed gasifier from the work of Schwitalla et al. [29]

$$2FeO + C = 2Fe + CO_2 \quad \text{(I)}$$

With the increasing temperature and residence time period, the zero valent iron reduced from the carbothermal reaction began to agglomerate into a particle with about 4 mm in diameter. The formation of the metallic iron would lead to a sudden increase of the slag viscosity, resulting in the blockage and shutdown of a gasifier [35].

The XRD spectra of the unmelted samples at different temperatures and different residence time periods are given in Fig. 4. When the residence time period was set to 30 min, minerals in the unmelted part were oldhamite (CaS), anhydrite ($CaSO_4$), calcite ($CaCO_3$), and hematite (Fe_2O_3) at 1300 ℃. When the temperature increased to 1350 ℃ or 1400 ℃, oldhamite (CaS), anhydrite ($CaSO_4$), and hematite (Fe_2O_3) were the main phases while calcite decomposed. Note that Fe_2O_3 mainly came from the oxidization of FeO by air during the sample treatment since FeO was no stable in the air. Furthermore, when the residence time period increased to 60 min, less peaks of anhydrite were found with the temperature increasing from 1300 to 1400 ℃. Oldhamite and hematite were the main minerals at higher temperature and longer residence time period. The residual carbon in the coal ash was proved to increase the ash fusion temperatures [36]. The interaction between the coal ash in the char particle and molten slag was inhibited, calcium was easy to react with sulfur in the coal ash, as shown in Table 2, and oldhamite and hematite formed during the migration process from the inside to the surface.

3.2. Carbon capacity of the molten slag

Fig. 5 shows the results of the mass ratio of the carbon that consumed by the molten slag to the total carbon in the coal char sample layer and the carbon capacity of the molten slag, which are calculated from Eqs. (11) and (12), at the conditions of different temperatures and residence time period. From Fig. 5a, the results showed that the mass ratio (w_c) increased with the temperature. When the set residence time period was 0 min and the slag temperature increased from 1300 ℃ to 1450 ℃, the mass ratio (w_c) increased from 25.6 wt% to 36.2 wt%. The mass ratio of the carbon that consumed by the molten slag the total carbon in the coal char sample layer displayed a 7.0 w.t% increment per 100 ℃ regardless of the residence time period, and currently this is only true for the investigated temperature range from 1300 to 1450 °C. At the same temperature, the increasing residence time period also increased the consumed mass ratio due to more residual carbon reacting with the molten slag. The increment of the consumed mass ratio per 1 h was about 11 wt% at the same temperature. These findings that the increasing consumed mass ratio with the residence time period and temperature mean more residual carbon reacted with the molten slag during the migration process.

To quantify the carbothermal reaction of the molten slag and

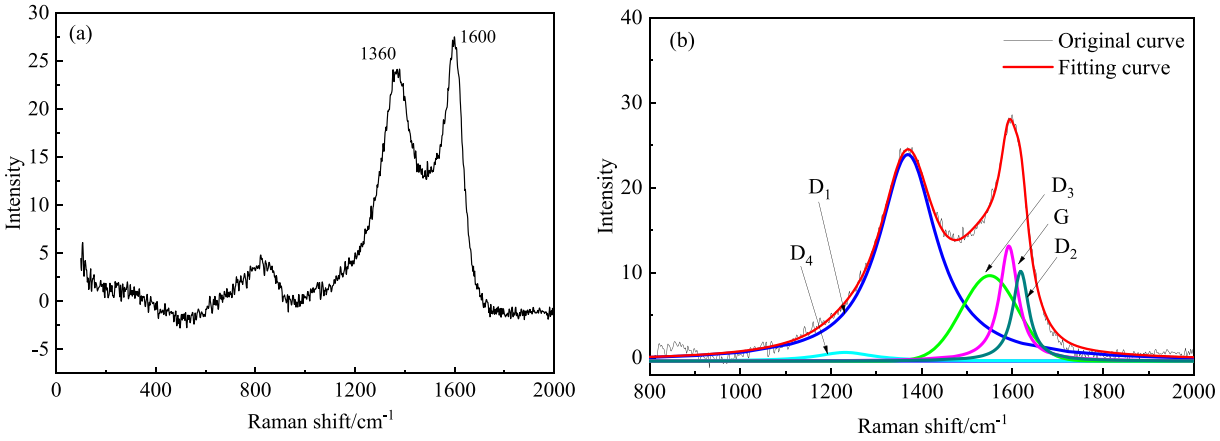

Fig. 6. Raman spectrum (a) and the peak fitting curves (b) of the coal char sample.

Table 4
First-order Raman bands, Raman shift, and vibration modes used in this study.

Band	Raman shift/ cm^{-1}	Vibration mode
/	227 293 411 612	α-Fe_2O_3 [38,39]
G	~1580	Ideal graphite lattice (E_{2g} symmetry) [40–42]
D1	~1350	Disordered graphitic lattice (graphene layer edges, A_{1g} symmetry) [40–42]
D2	~1620	Disordered graphitic lattice (surface graphene layers, E_{2g}-symmetry) [41]
D3	~1500	Amorphous carbon [42]
D4	~1200	Disordered graphitic lattice (A_{1g} symmetry), polyenes, ionic impurities [42]

residual carbon, a carbon capacity (I_c) was defined in this study and the results are given in Fig. 5b. When the residence time period was 0 min and the temperature was 1300 ℃, the carbon capacity of the molten slag was 0.024 kg/kg, indicating that about 0.024 kg residual carbon could react or leave in the 1 kg molten slag. This value increased with the residence time period and temperature. When the residence time period was set to constant, the carbon capacity increased from 0.024 to 0.033 kg/kg from 1300 to 1450 ℃ at the residence time period of 0 min. When the residence time period was 60 min, I_c could increase from 0.034 to 0.044 kg/kg from 1300 to 1450 ℃. However, when the slag temperature was set to constant, for instance, at 1400 ℃, the carbon capacity of the molten slag increased from 0.030 to 0.039 kg/kg. More residual carbon reacted with the molten slag at higher temperature via the carbothermal reaction. For an entrained flow gasifier with coal consumption of more than 2000 TPD, the captured amount of coal/char particles on the slag wall was predicted and accounted for about 55.4% of the total injected coal [6]. Thus, according to the quantitative research results in this study, the carbon capacity of the molten slag reflected that the chemical composition of the slag changed during the carbon migration process, which was also proved in the Ref. [37] that caused the transformation of the viscosity-temperature property.

3.3. *Effect of slag temperature*

The effects of slag temperature on the structure evolution of the residual carbon during the migration process and the carbothermal reaction were investigated by using Raman spectroscopy. The Raman spectrum of XLT coal char is given in Fig. 6a. In order to obtain more information about the structural evolutions of coal char and residual

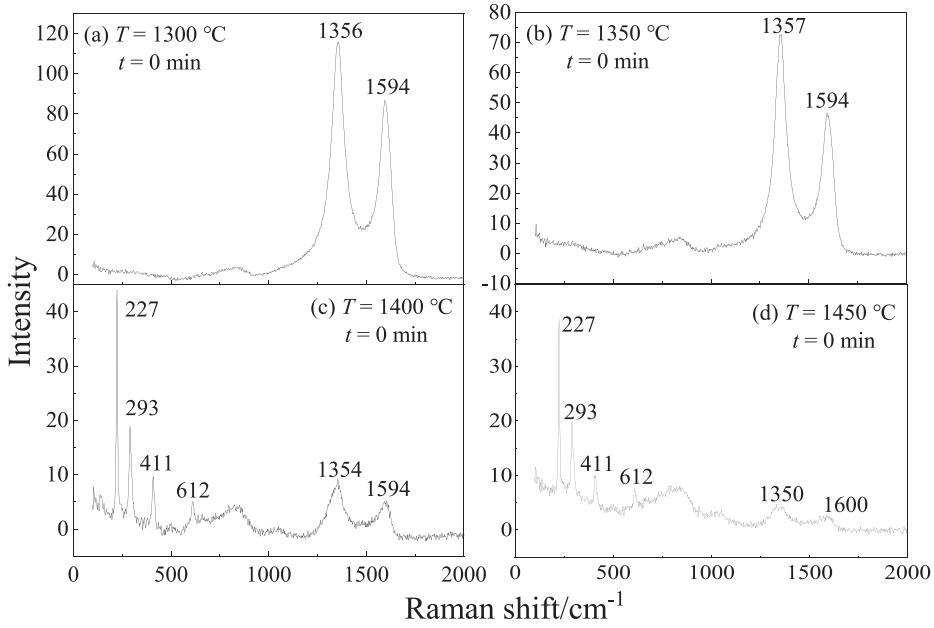

Fig. 7. Raman spectra of coal slag samples at different temperatures.

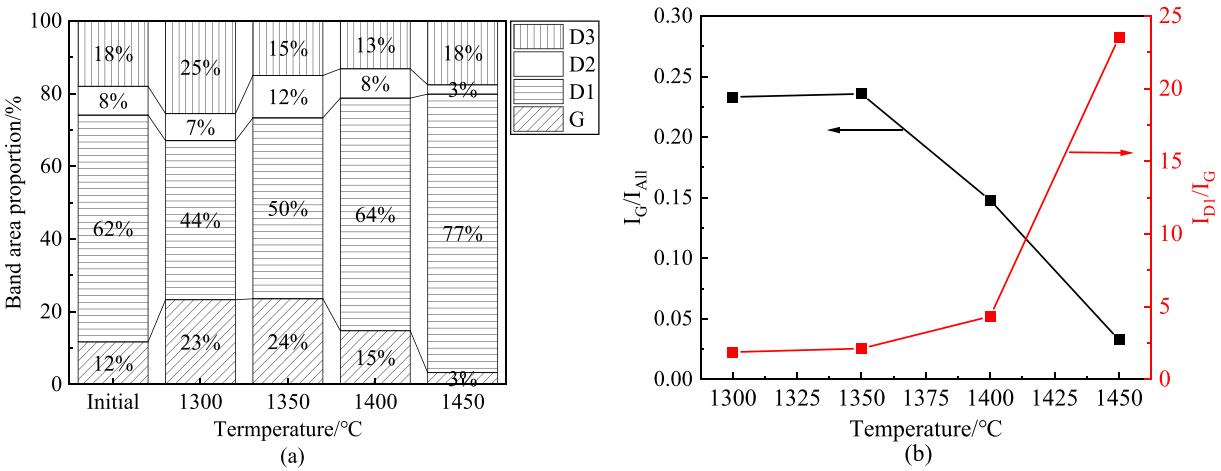

Fig. 8. The band area proportion (a) and ratio of peak integral area (b) at different temperatures.

carbon during the migration process, peak fitting with Gaussian or Lorentzian line shape for the original Raman spectrum was performed and shown in Fig. 6b. Parameters such as peak position, bands, Raman shift, and vibration modes used in this study are shown in Table 4. In Fig. 6a, two peaks, corresponding to the Raman shifts of 1360 and 1600 cm^{-1}, were tested. The first peak (1360 cm^{-1}) indicated the carbon structure was close to the overlapping peaks of D1 and D4 bands, which was disordered graphitic lattice with graphene layer edges and A_{1g} symmetry. The other one (1600 cm^{-1}) was close to the overlapping peaks of D2, D3, and G bands, which mainly were ideal graphite lattice with E_{2g} symmetry and disordered graphitic lattice. Generally, when the pyrolysis temperature was higher than 1200 ℃, the graphitization transformation occurs due to the transformation of amorphous carbon structure and defect structure into ordered crystal sp^2 carbon atom, and the I_{D1}/I_G significantly decreases and I_G/I_{All} significantly increases. In the Raman spectrum of Fig. 6a, the intensity of the peak (1600 cm^{-1}) was higher than the peak (1360 cm^{-1}), indicating that more approximated graphite structure formed during the pyrolysis process.

The original Raman spectra of coal slag samples at different temperatures when the residence time periods were set to 0 min are shown in Fig. 7. At 1300 ℃, two peaks with Raman shifts of 1356 and 1594 cm^{-1} were tested and shown in Fig. 7a while similar results were found in Fig. 7b at the temperature of 1350 ℃. However, when the temperature increased to 1400 ℃ or 1450 ℃, more peaks were tested, extra including the Raman shifts of 227, 293, 411, and 612 cm^{-1}. The Raman shifts (227, 293, 411, and 612 cm^{-1}) in Fig. 7c and 7d denoted the structure of iron oxides, which was α-Fe_2O_3. In the reducing atmosphere, iron exists as ferrous ionic (Fe^{2+}) in the molten slag [43]. Due to its instability at low temperature, it is easy to be oxidized into Fe^{3+} in air. During the sample treatment process, the contact with air cannot be avoided and resulted in the oxidation of the sample. In addition, the ratio of Fe^{3+} to Fe^{2+} increased significantly with the increase of oxygen partial pressure in slag [44,45]. Therefore, Fe_2O_3 appeared in the Raman spectra of this study. The formation of the iron oxide was mainly from the reoxidation of metallic iron reduced by the carbothermal reaction during the migration process. The peak positions at the Raman shifts of ~ 1350 and ~ 1600 cm^{-1} were both found in Fig. 7c and 7d. However, the intensities of these two peaks were much smaller than the values in Fig. 7a and 7b. With increasing temperature, the intensities of the peak at Raman shifts of ~ 1350 and ~ 1600 cm^{-1} decreased. From Table 4, it

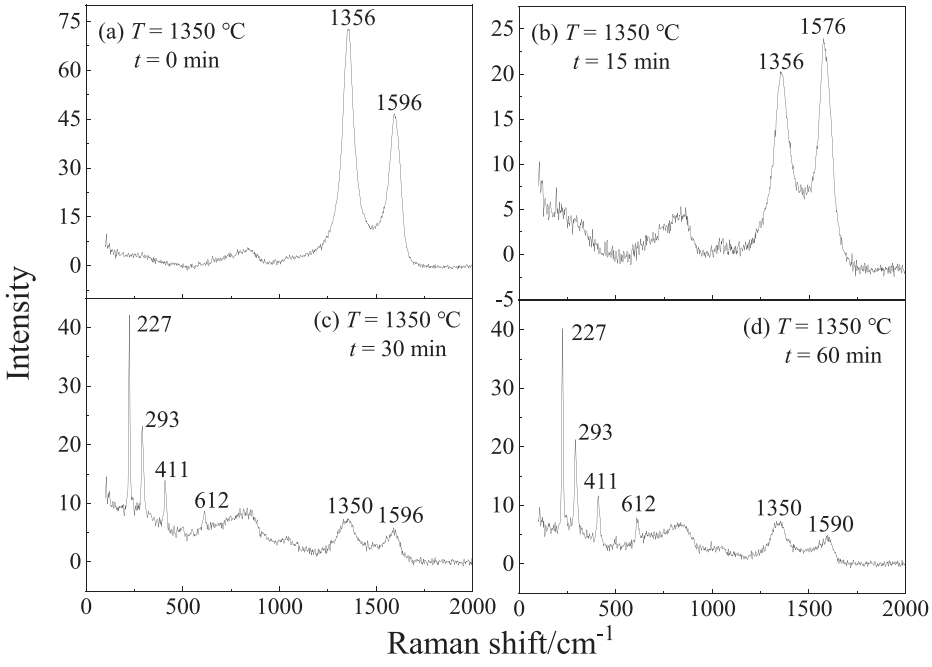

Fig. 9. Raman spectra of coal slag samples at different residence time periods.

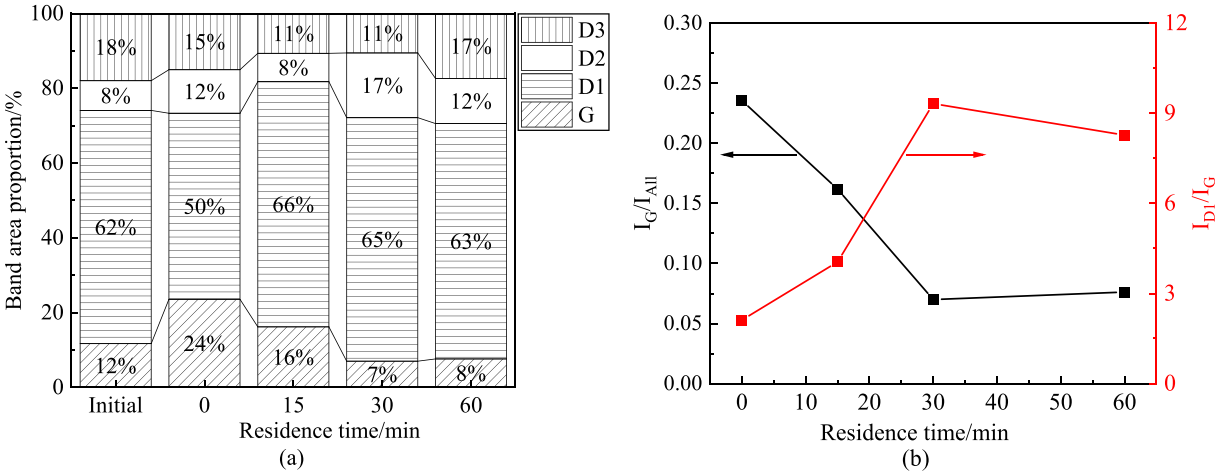

Fig. 10. The band area proportion (a) and ratio of the peak integral area (b) at different residence time.

was concluded that these two peaks were correspond to the carbon structure with ideal or disordered graphite lattice.

To study the structure evolution of the residual carbon at different temperatures, the band area proportion was calculated and the results are given in Fig. 8a. Compared to the initial structure of the char particle, G band proportion increased when the char particle was embedded in the molten slag layer while the D1 band proportion decreased. After the char particle was embedded in the molten slag, the area proportion of D1 band increased with the slag temperature, meaning a further carbon structure evolution occurred in the slag layer. This means that before the carbon in the char particle started to react with the slag, the carbon structure would change to graphite lattice structure and the disordered graphitic lattice decreased. Results showed that there were D1, D2, D3 and G bands in Raman peak fitting results. However, no D4 band was found in the fitting result, indicating that polyenes, and ionic impurities transformed to other carbon structure in the environment of high-temperature molten slag. The area proportion of D1 band as the defect band increased while this proportion of G band decreased with the temperature. This indicated that the structure of the residual carbon transformed from the ideal graphite lattice to disordered graphitic lattice, heterocyclic atom, and graphite defect with the increase of the slag temperature. The proportion as I_G/I_{All} of the ideal graphite structure in the total structure gradually decreased, which is shown in Fig. 8b. In addition, I_{D1}/I_G increased with the increase of temperature, indicating that the carbon microcrystalline structure in the residual carbon was destroyed at high temperature. This destroy of the graphitic lattice mainly came from the carbothermal reaction with molten slag at high temperature, such as the reaction between C with FeO. Then, small size microcrystalline structure was generated, which proved that the order of residual carbon structure reduced during the migration process.

3.4. Effect of residence time

The original Raman spectra of coal slag samples at 1350 ℃ with the variable of residence time period are shown in Fig. 9. Comparing the results in Figs. 7 and 9, similar results were found that peaks at the Raman shifts of ~ 1356 and ~ 1596 cm^{-1} at 0 min and ~ 1350 and ~ 1600 cm^{-1} at 15 min were tested. However, when the residence time period increased to 30 or 60 min, more peaks, including the Raman shifts of 227, 293, 411, and 612 cm^{-1} were shown in the Raman spectra. The iron oxides were formed when the residence time period was prolonged during the migration process. Besides, both peak positions at the Raman shifts of ~ 1350 and ~ 1600 cm^{-1} were tested as well and shown in Fig. 9c and 9d. The intensities of these two peaks at prolonged residence time period were much smaller than the peaks in Fig. 9a and 9b. The residual carbon was consumed via the carbothermal reaction and the structure was changed from graphitic lattice to disordered graphitic lattice during this process. The results indicated that the prolonged residence time period promote the carbothermal reaction and lead the structure evolution of the residual carbon in the molten slag.

In addition, the band area proportion and ratio of the peak integral area at different residence time periods was analyze via peak fitting. The results are shown in Fig. 10. Compared to the initial structure of the char particle, G band proportion increased at the beginning when the char particle was embedded in the molten slag layer while the D1 band proportion decreased. After that, the area proportion of D1 band increased with the residence time. This also indicated that a further carbon structure evolution occurred in the slag layer. The D1 band area proportion first increased from 50% to 66% when the residence time period increased to 15 min, and then it decreased to 65% and 63% at the residence time period of 30 min and 60 min, respectively. The intensity of D1 band was higher than that of other D bands, indicating that the residual carbon structure exists mainly in the form of disordered graphitic lattice. However, the G band area proportion decreased from 24% to 8% when the residence time period increased from 0 min to 60 min. The G band denoted the ideal graphite lattice while D1 and D2 mean the disordered graphitic lattice and D3 was amorphous carbon. The proportion as I_G/I_{All} of the ideal graphite structure in the total structure gradually decreased, which is shown in Fig. 10b. Thus, the result in Fig. 10a shows that the increasing residence time period lead the structure of the residual carbon to be transformed from graphitic structure to disordered structure or amorphous phase. The distribution of disordered graphitic lattice was not regular like the structure evolution shown in Fig. 8a. Furthermore, I_{D1}/I_G first increased and then decreased with the increase of the residence time period. With the increasing residence time period, the carbon structure corresponding to the D1 band transformed to another structure, such as amorphous carbon (D3 band). Therefore, the order of residual carbon structure decreased and the disordered structures transformed into each other with the increase of the residence time period. It was proved that the graphitization degree of residual carbon was not conducive to the occurrence of the carbon thermal reaction [16]. With the increase of the residence time period, the disordered degree of the residual carbon increased, which promoted the occurrence of the carbothermal reaction. Moreover, the effect of reaction temperature on the structure of carbon is greater than that of reaction time.

3.5. Slag transformation with carbon migration

During the migration process of the carbon in the slag layer, the carbothermal reaction consumed oxygen and changed the chemical composition of the slag, which would affect the slag transformation and

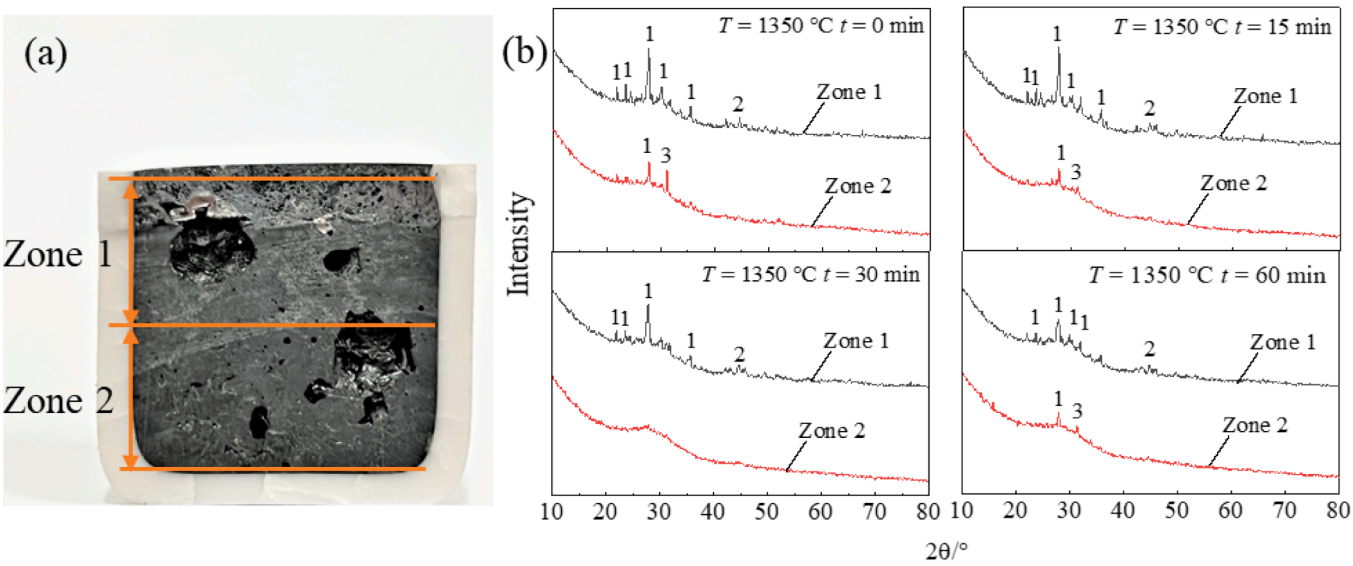

Fig. 11. The zone division of the slag layer (a) and XRD spectra (b) of the slag samples in two zones (Zone 1 and Zone 2) at different residence time periods when the temperature was 1350 ℃. (1-Labradorite ($NaAlSi_3O_8$-$CaAl_2Si_3O_8$), 2-metallic Fe (Fe), 3-Akermanite ($Ca_2Mg(Si_2O_7)$).

viscosity-temperature property. The slag transformation with the effects of the carbon migration and the carbothermal reaction was studied, and the XRD spectra for analyzing the mineral transformation are given in Fig. 11. In Fig. 11a, the cross section of the slag in the crucible was divided into two zones, namely zone 1 and zone 2, according to the position of the char particle layer shown in Fig. 1. Zone 1 was the migration zone of the char particle or residual carbon, and zone 2 was the slag zone without carbon inside. The results of Fig. 11b showed that the carbon migration and carbothermal reaction affected the intensity and number of peaks. In addition, it was found that the intensity and number of peaks decreased with the increase of reaction time. The slag in zone 1 contained labradorite ($NaAlSi_3O_8$-$CaAl_2Si_3O_8$) and metallic Fe while the slag of zone 2 has less content of labradorite ($NaAlSi_3O_8$-$CaAl_2Si_3O_8$) and a new phase (Akermanite ($Ca_2Mg(Si_2O_7)$) was formed. No metallic Fe was found in the XRD spectrum of the slag in zone 2. When the temperature was 1350 ℃ and the residence time period increased from 0 to 60 min, mineral types in both zones 1 and 2 were not changed. This indicated that the migration behavior and structure evolution of the residual carbon and the carbothermal reaction of the carbon significantly affected the slag transformation in the entrained flow gasifier. It was possible that the residual carbon in the slag acted as a crystal nucleus to promote the formation of the crystalline phase in the molten slag layer. For this observation, a comparison without the char layer would be good for the slag discharge of an entrained flow gasifier.

4. Conclusion

The migration and structure evolution of the carbon in the molten slag layer and its effect on the slag transformation was investigated in this study. The results showed that the carbon migrated upward to the molten slag surface due to the lower density and porous structure. During the migration process, the carbon reacted with the iron oxide via carbothermal reaction and produced metallic iron enclosures on the interface between the unmelted particle layer and slag. The structure of the metallic iron enclosure transformed from laminar shape to spherical structure. The mass ratio of the carbon that consumed by the molten slag, including the carbon via carbothermal reaction and remain as residual carbon, to the total carbon of the char sample layer increased with the increases of the temperature and residence time. Besides, the carbon capacity of the molten slag and the disordered degree of the residual carbon structure increased. However, the graphitic structure of the residual carbon in the molten slag layer decreased with slag temperature and residence time. The increasing degree of the disordered structure of the residual carbon would promote the occurrence of the carbothermal reaction. Finally, it was proved that the migration and structure evolution of the carbon promoted the crystallization behavior. The molten slag formed more labradorite inside the layer, which should be considered for the prediction of the viscosity-temperature of the coal slag during the entrained flow gasification process.

CRediT authorship contribution statement

Xiaodan Bao: Resources, Data curation, Formal analysis, Investigation, Methodology, Software, Visualization, Writing – original draft, Writing – review & editing. **Ming Gong:** Resources, Data curation, Formal analysis, Investigation, Methodology, Software, Visualization, Writing – review & editing. **Zhongjie Shen:** Conceptualization, Supervision, Formal analysis, Methodology, Software, Project administration, Funding acquisition, Writing – original draft, Writing – review & editing. **Jianliang Xu:** Conceptualization, Resources, Data curation, Formal analysis, Software, Writing – original draft, Writing – review & editing. **Qinfeng Liang:** Conceptualization, Validation, Resources, Investigation, Methodology, Writing – review & editing. **Haifeng Liu:** Conceptualization, Supervision, Validation, Formal analysis, Methodology.

Declaration of Competing Interest

The authors declare that they have no known competing financial interests or personal relationships that could have appeared to influence the work reported in this paper.

Acknowledgements

This study was sponsored by the National Natural Science Foundation of China (Grant No.21908063), the Shanghai Pujiang Program (21PJ1402300) and the Fundamental Research Funds of the Central Universities (JKB01211715).

References

[1] Higman C, Tam S. Advances in coal gasification, hydrogenation, and gas treating for the production of chemicals and fuels. Chem Rev 2014;114(3):1673–708.
[2] Gong X, Lu W, Guo X, Dai Z, Liang Q, Liu H, et al. Pilot-scale comparison investigation of different entrained-flow gasification technologies and prediction on industrial-scale gasification performance. Fuel 2014;129:37–44.

[3] Ünlü A, Kayahan U, Argönül A, Ziypak M, Akça A. Pilot scale entrained flow gasification of Turkish lignites. J Energy Inst 2017;90(1):159–65.
[4] Liu M, Shen Z, Liang Q, Xu J, Liu H. New Slag–char Interaction mode in the later stage of high ash content coal char gasification. Energy Fuels 2018;32(11):11335–43.
[5] Li S, Wu Y, Whitty KJ. Ash deposition behavior during char-slag transition under Simulated Gasification Conditions. Energy Fuels 2010;24(3):1868–76.
[6] Xu J, Liang Q, Dai Z, Liu H. Comprehensive model with time limited wall reaction for entrained flow. Fuel 2016;184:118–27.
[7] Ni J, Yu G, Guo Q, Zhou Z, Wang F. Submodel for predicting slag deposition formation in slagging gasification systems. Energy Fuels 2011;25(3):1004–9.
[8] Safronov D, Förster T, Schwitalla D, Nikrityuk P, Guhl S, Richter A, et al. Numerical study on entrained-flow gasification performance using combined slag model and experimental characterization of slag properties. Fuel Process Technol 2017;161:62–75.
[9] Montagnaro F, Salatino P. Analysis of char–slag interaction and near-wall particle segregation in entrained-flow gasification of coal. Combust Flame 2010;157(5):874–83.
[10] Montagnaro F, Brachi P, Salatino P. Char-wall interaction and properties of slag waste in entrained-flow gasification of coal. Energy Fuels 2011;25(8):3671–7.
[11] Shen Z, Liang Q, Xu J, Zhang B, Liu H. In-situ experimental study of CO_2 gasification of char particles on molten slag surface. Fuel 2015;160:560–7.
[12] Shen Z, Liang Q, Xu J, Zhang B, Han D, Liu H. In situ experimental study on the combustion characteristics of captured chars on the molten slag surface. Combust Flame 2016;166:333–42.
[13] Liu M, Shen Z, Liang Q, Xu J, Liu H. In situ experimental study of CO_2 gasification of petcoke particles on molten slag surface at high temperature. Fuel 2021;285:119158. https://doi.org/10.1016/j.fuel.2020.119158.
[14] Li P, Yu Q, Xie H, Qin Q, Wang K. CO_2 gasification rate analysis of datong coal using slag granules as heat carrier for heat recovery from blast furnace slag by using a chemical reaction. Energy Fuels 2013;27(8):4810–7.
[15] Kong L, Bai J, Li W, Wen X, Liu X, Li X, et al. The internal and external factor on coal ash slag viscosity at high temperatures, Part 2: Effect of residual carbon on slag viscosity. Fuel 2015;158:976–82.
[16] Wang Ji, Kong L, Bai J, Li H, Bai Z, Li X, et al. The role of residual char on ash flow behavior, Part 1: The effect of graphitization degree of residual char on ash fusibility. Fuel 2018;234:1173–80.
[17] Chen D-X, Tang L-H, Zhou Y-M, Wang W-M, Wu Y-Q, Zhu Z-B. Effect of char on the melting characteristics of coal ash. J Fuel Chem Technol 2007;35(2):136–40.
[18] Wu S, Huang S, Ji L, Wu Y, Gao J. Structure characteristics and gasification activity of residual carbon from entrained-flow coal gasification slag. Fuel 2014;122:67–75.
[19] Wu T, Gong M, Lester Ed, Wang F, Zhou Z, Yu Z. Characterisation of residual carbon from entrained-bed coal water slurry gasifiers. Fuel 2007;86(7-8):972–82.
[20] Wang Ji, Kong L, Bai J, Xue K, Zhu X, Luo Y, et al. Characterization of slag from anthracite gasification in moving bed slagging gasifier. Fuel 2021;292:120390. https://doi.org/10.1016/j.fuel.2021.120390.
[21] Ma Z, Bai J, Li W, Bai Z, Kong L. Mineral transformation in char and its effect on coal char gasification reactivity at high temperatures, part 1: mineral transformation in char. Energy Fuels 2013;27(8):4545–54.
[22] Ma Z, Bai J, Wen X, Li X, Shi Y, Bai Z, et al. Mineral transformation in char and its effect on coal char gasification reactivity at high temperatures part 3: carbon thermal reaction. Energy Fuels 2014;28(5):3066–73.
[23] Wang J, Ishida R, Takarada T. Carbothermal reactions of quartz and kaolinite with coal char. Energy Fuels 2000;14(5):1108–14.
[24] Wang Ji, Kong L, Bai J, Zhao H, Guhl S, Li H, et al. The role of residual char on ash flow behavior, Part 2: Effect of SiO_2/Al_2O_3 on ash fusibility and carbothermal reaction. Fuel 2019;255:115846. https://doi.org/10.1016/j.fuel.2019.115846.
[25] Wang Ji, Kong L, Bai J, Zhao H, Xue K, Zhu X, et al. The role of residual char on ash flow behavior, Part 3: Effect of Fe_2O_3 content on ash fusibility and carbothermal reaction. Fuel 2020;280:118705. https://doi.org/10.1016/j.fuel.2020.118705.
[26] Van Dyk JC, Benson SA, Laumb ML, Waanders B. Coal and coal ash characteristics to understand mineral transformations and slag formation. Fuel 2009;88(6):1057–63.
[27] Pan C, Liang Q, Guo X, Dai Z, Liu H, Gong X. Characteristics of different sized slag particles from entrained-flow coal gasification. Energy Fuels 2016;30(2):1487–95.
[28] Xu S, Zhou Z, Gao X, Yu G, Gong X. The gasification reactivity of unburned carbon present in gasification slag from entrained-flow gasifier. Fuel Process Technol 2009;90(9):1062–70.
[29] Schwitalla DH, Guhl S, Laabs M, Reinmöller M, Bai J, Meyer B. Thermochemical and analytical approach to describe secondary slag phase formation and local process conditions in a full-scale BGL gasifier. Fuel Process Technol 2021;217:106833. https://doi.org/10.1016/j.fuproc.2021.106833.
[30] Bale CW, Bélisle E, Chartrand P, Decterov SA, Eriksson G, Gheribi AE, et al. FactSage thermochemical software and databases, 2010–2016. Calphad 2016;54:35–53.
[31] Reinmöller M, Klinger M, Schreiner M, Gutte H. Relationship between ash fusion temperatures of ashes from hard coal, brown coal, and biomass and mineral phases under different atmospheres: A combined FactSage™ computational and network theoretical approach. Fuel 2015;151:118–23.
[32] Locock AJ, Chesterman D, Caird D, Duke MJM. Miniaturization of mechanical milling for powder X-ray diffraction. Powder Diffract 2012;27(3):189–93.
[33] Schwitalla DH, Bronsch AM, Klinger M, Guhl S, Meyer B. Analysis of solid phase formation and its impact on slag rheology. Fuel 2017;203:932–41.
[34] Spasic AM. Rheology of emulsions. Chapter 1 - Introduction. Interface Science and Technology 2018;22:1-25.
[35] He C, Bai J, Kong L-X, Guhl S, Schwitalla DH, Xu J, et al. The precipitation of metallic iron from coal ash slag in the entrained flow coal gasifier: By thermodynamic calculation. Fuel Process Technol 2017;162:98–104.
[36] Wu H, Zhang Y, Ren Q, Wang Ya, Lyu Q. Impact of residual carbon on ash Fusibility of semi-char from an industrial circulating fluidized bed gasifier. Energy Fuels 2019;33(1):531–40.
[37] Vargas S, Frandsen FJ, Dam-Johansen K. Rheological properties of high-temperature melts of coal ashes and other silicates. Prog Energy Combust Sci 2001;27(3):237–429.
[38] De Faria DLA, Venâncio Silva S, De Oliveira MT. Raman microspectroscopy of some iron oxides and oxyhydroxides. J. Raman Spectrosc 1997;28:873–8.
[39] Thibeau RJ, Brown CW, Heidersbach RH. Raman spectra of possible corrosion products of iron. Appl Spectrosc 1978;32(6):532–5.
[40] Tuinstra F, Koenig JL. Raman spectrum of graphite. J Chem Phys 1970;53(3):1126–30.
[41] Wang Y, Alsmeyer DC, McCreery RL. Raman spectroscopy of carbon materials: structural basis of observed spectra. Chem Mater 1990;2(5):557–63.
[42] Sadezky A, Muckenhuber H, Grothe H, Niessner R, Pöschl U. Raman micro spectroscopy of soot and related carbonaceous materials: Spectral analysis and structural information. Carbon 2005;43(8):1731–42.
[43] Obiso D, Schwitalla DH, Korobeinikov I, Meyer B, Reuter M, Richter A. Dynamics of rising bubbles in a quiescent slag bath with varying thermo-physical properties. Metallurgical and Materials Transactions 2020;51(6):2843–61.
[44] Kimura H, Endo S, Yajima K, Tsukihashi F. Effect of oxygen partial pressure on liquidus for the $CaO–SiO_2–FeO_x$ system at 1573 K. ISIJ Int 2004;44(12):2040–5.
[45] Bogdandy LV, Engell HJ. The Reduction of Iron Ores. Scientific Basis and Technology. Berlin: Springer; 1971.